**DOI 10.31489/2021No2/6-11**

**UDC 537.622.3, 537.622.4, 539.611, 544.011, 544.226**

# ON THE TRANSITION BETWEEN FERROMAGNETIC AND PARAMAGNETIC STATES IN MESOPOROUS MATERIALS WITH FRACTAL MORPHOLOGY

**Shishulin A.V.[1,*], Potapov A.A.[2,3], Shishulina A.V.[4,5]**

[1]G.A. Razuvaev institute of organometallic chemistry, Russian Academy of sciences, Nizhny Novgorod, Russia, chichouline_alex@live.ru

[2]V.A. Kotel'nikov institute of radio engineering and electronics, Russian Academy of sciences, Moscow, Russia

[3]JNU-IREE RAS Joint Laboratory of Information Technology and Fractal Processing of Signals, Jinan University, Guangzhou, China

[4]R.E. Alekseev Nizhny Novgorod State technical University, Nizhny Novgorod, Russia

[5]N.I. Lobachevsky Nizhny Novgorod State University, Nizhny Novgorod, Russia

*In this paper, we have shown how the presence of pores and pore morphology influence on magnetic phase transition temperatures in mesoporous ferromagnetic materials. Model calculations have demonstrated the possibility to obtain macroscopic mesoporous samples with notably reduced Curie temperatures which is also further depressed in the case the pore morphology is more complicated. The results have been obtained on the basis of the experimentally verified correlation between the Curie temperature and cohesive energy of the material and illustrated using the examples of pure mesoporous iron, nickel and cobalt while pore morphology has been determined by the methods of fractal geometry. Several practical applications of mesoporous materials with tuned values of the Curie temperature have also been discussed in the final section.*

***Keywords:*** mesoporous materials, second-order phase transition, ferromagnetism, Curie temperature, cohesive energy.

## Introduction

Nanostructured ferromagnetic materials are objects of a considerable interest among researchers [1]. Tremendous attention is being attracted to such materials in recent years due to a wide range of their technological applications including high-density information storage devices [2], magneto-optical sensors [3], spintronics devices [4], biomedical technologies [5] etc, as well as a set of phenomena of fundamental interest such as superparamagnetism [6], giant magnetoresistance [7, 8], complicated dynamics of magnetic skyrmions [9] or magnetic catalysis [10]. One of the main and vital parameters which determine the behavior of ferromagnetic materials is the Curie temperature (temperature of a second-order phase transition when magnetic ordering disappears and ferromagnetic materials become paramagnetic). It is well-known that nanoscale particles or grains of a ferromagnetic material exhibit a lower Curie temperature [11-20] which is (as well as some other parameters, e.g. the saturation magnetization [16], characteristics of hysteresis loops [20] or magnetic anisotropy constants [21]) size- [11-20] and shape-dependent [14,15,20]. Such size- and shape effects in nanoparticles are commonly related to an increase in the surface-to-volume ratio with decreasing the size of a nanoparticle and "complicating" its shape which causes an increase in the fraction of lower coordinated atoms near the surface edge with magnetic characteristics (e.g. magnetic moments, exchange integrals etc. [19]) different from the bulk ones. Such regularities could be described using various approaches including models based on the spin-spin correlation length mechanism [11], on the bond order-length-strength correlation combined with the Ising preposition [12],on Monte-Carlo [19,20] and molecular-statics simulations on the Ising model [20] or on the size- and shape-dependent cohesive energy of nanostructures [14-16].

Note that high surface-to-volume ratios and fractions of surface atoms could be obtained not only in nanopowders or in nanocomposites containing nanoparticles distributed in a matrix, but also in microporous and mesoporous materials, while porous samples of such materials can be macroscopic-sized [22-24]. Formation of such structures is possible, for example, during the early stages of spark plasma sintering [25],

laser sintering [26] of nanopowders (a review of synthesis methods of nanosized powders has been presented by M.K. Berner *et al* [27]) as well as using a variety of other techniques, e.g. [28].

## 1. A cohesive energy-based model for magnetic phase transitions in mesoporous media.

The object of simulation is a mesoporous material with the given volume fraction of pores, $\alpha$. In order to take into account possible irregular and complicated pore shapes [28], let us introduce two parameters for their description. The first one is the effective diameter of the pore, $d_{eff}$, which is equal to the diameter of a spherical pore of the same volume, and the second one could be, for example, the pore shape coefficient, $k$. The shape coefficient is the ratio between the surface area of the pore under consideration, $A$, and the surface area of the sphere of the same volume, $A_0$: $k = A/A_0$ (in details, such approach and its variants have been described in [29-32], being applied to porous structures. In [33], some other geometry considerations could be found). The number of pores in 1 g of a material, $N_{por}$, could be calculated as $N_{por} = 6\alpha \cdot 1\,\mathrm{g} \big/ \left(\pi\rho d_{eff}^3\right)$ where $\rho$ is the material density. Factor 1 g has been introduced to match the units. The specific surface area, $A_{sp}$, could be expressed as $A_{sp} = N_{por} \cdot \pi k d_{eff}^2 = 6\alpha k \cdot 1\,\mathrm{g} \big/ \left(\rho d_{eff}\right)$. To estimate the influence of the pore morphology on the Curie temperature of a mesoporous material, let us use a simple expression describing the relation between the Curie temperature of a material and its cohesive energy:

$$\frac{T_c^{por}}{T_c^{bulk}} = \frac{E_{coh}^{por}}{E_{coh}^{bulk}}. \tag{1}$$

Here, $E_{coh}^{por}$ and $E_{coh}^{bulk}$ are the cohesive energies of porous and continuous materials, respectively; $T_c^{por}$ and $T_c^{bulk}$ are the Curie temperatures of a porous material and a material in the absence of pores, respectively.

This expression has been retrieved in Refs. [13-16] and experimentally justified by the authors of [16]. This expression is similar to the one used by G. Guisbiers, *et al* to describe different size-and shape-dependent material properties [34-36] and also found to be in a good agreement with experimental data. 1g of a porous material contains $N$ atoms, where $N = 6\omega \cdot 1\,\mathrm{g} \big/ \left(\pi d_{at}^3 \cdot \rho\right)$. Here, $d_{at}$ is the atomic diameter and $\omega$ is the lattice packing parameter in the crystal structure. $N_s$ atoms are located on the pore walls: $N_s = \eta A_{sp} \big/ \pi d_{at}^2 = 6\alpha\eta k \cdot 1\,\mathrm{g} \big/ \left(\pi\rho d_{at}^2 d_{eff}\right)$ where $\eta$ is the surface packing parameter. So, the number of atoms at the surface is given by

$$N_s = \left(\frac{6 \cdot 1\,\mathrm{g}}{\pi\rho}\right)^{1/3} \cdot \frac{\alpha\eta k}{\omega^{2/3} d_{eff}} N^{2/3}. \tag{2}$$

The estimates for the cohesive energy of a porous material could be obtained using the relations suggested by F. Aqra and A. Ayyad [37]:

$$\begin{aligned} E_{coh}^{bulk} &= \frac{1}{2}\beta N \varepsilon_b, \\ E_{coh}^{por} &= \frac{1}{2}\beta\varepsilon_b \left(\frac{1}{4}N_s + \left(N - N_s\right)\right), \end{aligned} \tag{3}$$

where $\beta$ is the number of bonds per one atom in the structure and $\varepsilon_b$ is the bond energy.

Therefore, from Eqs. (1-3) we have

$$E_{coh}^{por} = \frac{1}{2}\beta\varepsilon_b N \left(1 - \frac{3}{4}\left(\frac{6 \cdot 1\,\mathrm{g}}{\pi\rho}\right)^{1/3} \frac{\alpha\eta k}{\omega^{2/3} d_{eff}} N^{-1/3}\right), \tag{4}$$

$$T_c^{por} = T_c^{bulk} \left(1 - \frac{3}{4}\left(\frac{6 \cdot 1\,\mathrm{g}}{\pi\rho}\right)^{1/3} \frac{\alpha\eta k}{\omega^{2/3} d_{eff}} N^{-1/3}\right). \tag{5}$$

Below, the Curie temperatures of mesoporous materials have been estimated by using Eq. 5. High values of shape coefficient $k$ could be obtained, for example, in the case of porous materials where the pores have the shapes similar to simple non-spherical geometric structures (for example, $k$=1.49 for a tetrahedron, $k$=1.52 for a cone, $k$=3.20 for a star icosahedron (an icosahedron with a tetrahedron at each face)) or structures extended in one direction (for example, values $k$>2.00 correspond to oblate spheroids with aspect ratio $a/b$>5 or to prolate spheroids with $a/b$>3). Moreover, high surface-to-volume ratios are also characteristic for pores of complicated and irregular shapes, in order to take into account their morphology, the notion of fractal geometry is often used [29,30,38-42]. According to the approach suggested by us in [30, 40-42], the shape of a pore can be characterized by its fractal dimension $D$ which correlates its volume $V$ and surface area $A$: $A = CV^{2/D}$, where $C$ is a numerical coefficient.

Without any losses of generality, coefficient $C$, which also matches dimensions, is accepted below to be $4\pi$ for the sake of convenience. For real irregular morphologies of materials structure elements, $D$<3 and is typically non-integer. The most classic examples of fractal structures are *worm-like*, *amoeba-like,* and *porcupine-like* ones [30, 40-43].

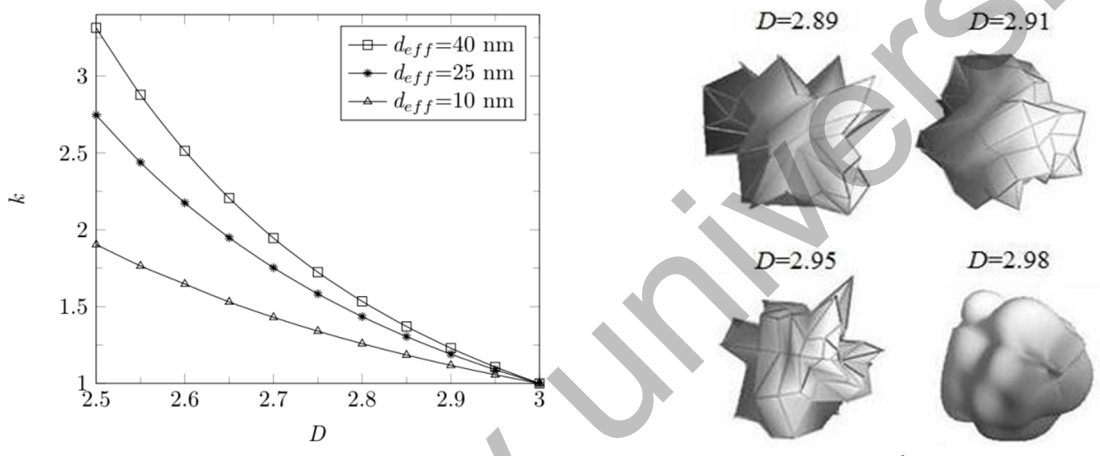


*a* *b*

**Fig. 1.** a) shape coefficient $k$ of a pore versus its effective diameter $d_{eff}$ and fractal dimension $D$; b) examples of "amoeba-like" and "porcupine-like" fractal structures with various $D$.

The correlation between shape coefficient $k$ (the ratio between the surface areas of the pore under consideration and the spherical pore of the same volume), pore volume $V = \pi d_{eff}^3/6$ and its fractal dimension $D$ is determined as follows: $k(V,D) = V^{2/D}/(3V/4\pi)^{2/3}$ (see Fig. 1a). Several examples of *amoeba-like* and *porcupine-like* structures with various fractal dimensions are presented in Fig. 2b.

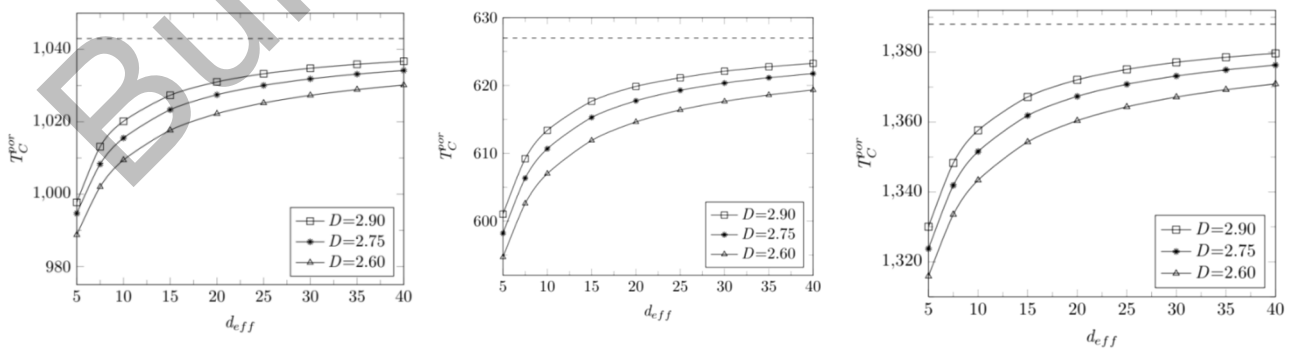


*a* *b* *c*

**Fig. 2.** The dependences of the Curie temperatures for mesoporous Fe (a), Ni (b), Co (c) on pore geometric characteristics (fractal dimensions $D$ and effective diameters $d_{eff}$ of pores). The Curie temperatures for continuous macroscopic samples are 1043 for Fe, 627 K for Ni,1388 K for Co.

It is necessary to note that such parameters as shape coefficients or fractal dimensions generalize different but equivalent variants of materials morphology: the structures which differ in their geometric outlook but share the same values of $k$ or $D$ (see Fig. 1b in [41], for example) have the same fraction of surface atoms and demonstrate the same behavior in the case considered in the present paper.

Specific surface areas in micro- and mesoporous materials can reach extremely high values (from 500$m^3$/g [22] to 1000 $m^3$/g [23] or even several thousands of $m^3$/g [24]). In the present paper, however, we limit ourselves to considering materials with not very high specific surface areas (in comparison with the values obtained in [22-24]), mostly below 200-300 $m^3$/g ($\alpha$=0.85). The dependences of the Curie temperature on pore size and shape for mesoporous iron (*a*), nickel (*b*) and cobalt (*c*) are plotted in Fig. 2. For these metals, material densities and atomic diameters are accepted in our estimates to be 7.874 g/$cm^3$ and 252 pm, respectively, for Fe; 8.902 g/$cm^3$ and 248 pm, respectively, for Ni; 8.900 g/$cm^3$ and 250 pm, respectively, for Co. The structure of nickel is *fcc* within the entire temperature range up to the melting point. At the same time, cobalt has two stable polymorphic modifications: β-Co with a *fcc* crystal lattice which is equilibrium in the considered temperature range and low-temperature hexagonal α-Co (the temperature of the α↔β polymorph transition is about 700 K). At the temperatures under consideration, the structure of Fe is *bcc* (α-Fe), iron exhibits the α↔γ polymorph transition between *bcc* and *fcc* modifications at about 1190 K. Packing parameters are $\omega$=0.74, $\eta$ = 0.91 for *fcc* structures [37,44] and $\omega$=0.68, $\eta$ = 0.83 for *bcc* ones [44].

Fig. 2 shows that reducing the effective pore diameter, $d_{eff}$, and increase the shape coefficient, $k$, (an increase in the specific surface area of a material) are accompanied with a decrease in the Curie temperature. Note that in the case of pores filled with a substance, such estimates are to be corrected, for example, by modifying the approach suggested by C. Ling-fei *et al*. [14] for embedded nanoparticles. Increasing the specific surface area of porous materials up to the values obtained experimentally by the authors of [22-24] allows expecting much more significant shifts of the magnetic transition temperatures similar to the ones obtained in [19] for free-standing nanoparticles.

## Conclusion

It is also worth noting that micro- and mesoporous materials (with functionalized pore walls [45], maybe) have a wide range of technological applications e.g. nanoreactor matrices [46]. For multiple applications, a great interest is attracted by magnetocaloric effects in ferromagnetic nanostructures, for example, heating ferromagnetic nanoparticles - invasive agents in alternating magnetic fields (magnetic hyperthermia treatment for cancer) due to hysteresis losses, losses for re-orientation of the magnetization vector etc. and maintaining their temperature near the Curie point [5, 47]. In the case considered in this paper, the possibility to tune the Curie temperature of materials by preparing the samples with different pore morphologies and specific surface areas shows possibilities to obtain mesoporous materials/nanoreactors with self-imposed limits of raising the temperature in alternating magnetic fields and the possibility of autonomous temperature control. The considered ferromagnetic materials have also high catalytic activity in a variety of commonly used chemical reactions [36]; meanwhile, materials with a higher specific surface area of pores (up to the ones from [24]) allow expecting a more significant decrease in the Curie temperatures down to the values demonstrated in [19].

## Acknowledgments

The research has been performed in the framework of the state task for IOMC RAS.

## REFERENCES

1 Binns C. (ed.) *Nanomagnetism: fundamentals and applications*. Newnes, Front. nanosc. 2014, 328 p.

2 Tannous C., Comstock R.L. *Magnetic information-storage materials.* In: Springer handbook of electronic and photonic materials. Cham, Springer. 2017, pp. 1185 – 1220. https://doi.org/10.1134/S1063776117010046.

3 Wang S.X., Li G.. Advances in giant magnetoresistance biosensors with magnetic nanoparticle tags: review and outlook. *IEEE trans. magn.* 2008, Vol. 44, pp. 1687 – 1702. https://doi.org/10.1109/TMAG.2008.920962.

4 Lashkarev G.V., Radchenko M.V., Bugaiova M.E., et.al. Ferromagnetic nanocomposites as spintronic materials with controlled magnetic structure. *Low temp. phys.* 2013, Vol. 39, No. 1, pp. 66–75. https://doi.org/10.1063/1.4776232.

5 Spirou S.V., Basini M., Lascialfari A., et al. Magnetic hyperthermia and radiationtherapy: radiobiological principles and current practice. *Nanomaterials.* 2018, Vol. 8, No. 401. https://doi.org/10.3390/nano8060401.

6 Mihaela O. Study about the possibility to control the superparamagnetism-superferromagnetism transition in magnetic nanoparticle systems. *J. magn. magn. mater.* 2013, Vol. 343, pp. 189 – 193. https://doi.org/10.1016/j.jmmm.2013.05.011.

7 Marrows C.H., Perez M., Hickey B.J. Finite size scaling effects in giant magnetoresistance multilayers. *J. phys.: condens. matter.* 2006, Vol. 18, No. 243. https://doi.org/10.1088/0953-8984/18/1/017.

8 Lobov I.D., Kirillova M.M., Romashev L.N., et al. Magnetorefractive effect and giant magnetoresistance in Fe($t_x$)/Cr superlattices. *Phys. solid state*. 2009, Vol. 51, No. 12, pp. 2337 – 2341. https://doi.org/10.1134/S1063783409120099.

9 Temiryazev A.G., Temiryazeva M.P., Zdoroveyshchev A.V., et al. Formation of a domain structure in multilayer CoPt films by magnetic probe of an atomic force microscope. *Phys. solid state*. 2018, Vol. 60, No. 11, pp. 2200 – 2206. https://doi.org/10.1134/S1063783418110318.

10 Filev V.G., Raskov R.C. Magnetic catalysis of chiral symmetry breaking: a holographic perspective. *Adv. high energy phys*. 2010, No. 473206. https://doi.org/10.1155/2010/473206.

11 Fisher M.E, Barber M.N. Scaling theory for finite-size effects in the critical region. *Phys. rev. lett.* 1972, Vol. 28, pp. 1516 – 1519. https://doi.org/10.1103/PhysRevLett.28.1516.

12 Sun C.Q., Zhong W.H., Li S., et al. Coordination imperfection suppressed phase stability of ferromagnetic, ferroelectric, and superconductive nanosolids. *J. phys.chem. B.* 2004, Vol. 108, pp. 1080 – 1084. https://doi.org/10.1021/jp0372946.

13 Yang C.C., Jiang Q. Size and interface effects on critical temperatures of ferromagnetic, ferroelectric and superconductive nanocrystals. *Acta mater.* 2005, Vol. 53, pp. 3305 – 3311. https://doi.org/10.1016/j.actamat.2005.03.039.

14 Ling-fei C., Dan X., Ming-xing G., et al. Size and shape effects on Curie temperature of ferromagnetic nanoparticles. *Trans. nonferrous met. soc. China.* 2007. Vol. 17, pp. 1451 – 1455. https://doi.org/10.1016/S1003-6326(07)60293-3.

15 Delavari H., Hosseini H.M., Simchi A. A simple model for the size- and shape-dependent Curie temperature of freestanding Ni and Fe nanoparticles based on the average coordination number and atomic cohesive energy. *J. chem. phys.* 2011, Vol. 383, pp. 1 – 5. https://doi.org/10.1016/j.chemphys.2011.03.010.

16 He X., Zhong W., Au C.-T., et al. Size dependence of the magnetic properties of Ni nanoparticles prepared by thermal decomposition method. *Nanoscale res. lett.* 2013, Vol. 8, No. 446. https://doi.org/10.1186/1556-276X-8-446.

17 Nikiforov V.N., Koksharov Yu.A., Polyakov S.N., et al. Magnetism and Verwey transition in magnetite nanoparticles in thin polymer film. *J. alloys compd*. 2013, Vol. 569, pp. 58 – 61. https://doi.org/10.1016/j.jallcom.2013.02.059.

18 Shuai Z., Li H. Size-dependent piezoelectric coefficient and Curie temperature of nanoparticles. *Nanomaterials and energy*. 2017, Vol. 6, No. 2, pp. 53 – 58. https://doi.org/10.1680/jnaen.16.00014.

19 Nikiforov V.N., Ignatenko A.N., Irkhin V.Yu. Size and surface effects on the magnetism of magnetite and maghemite nanoparticles. *J. exp. theor. phys.* 2017, Vol. 124, No. 2, pp. 304 – 310. https://doi.org/10.1134/S1063776117010046.

20 Essajai R., Benhouria Y., Rachadi A., et al. Shape-dependent structural and magnetic properties of Fe nanoparticles studied through simulation methods. *RSC adv*. 2019, Vol. 9, pp. 22057 – 22063. https://doi.org/10.1039/C9RA03047F.

21 Stolyar S.V., Komogortsev S.V., Chekanova L.A., et al. Magnetite nanocrystals with a high magnetic anisotropy constant due to the particle shape. *Tech. phys. lett.* 2019, Vol. 45, No. 9, pp. 878 – 881. https://doi.org/10.1134/S1063785019090116.

22 Gaev D.S., Rekhviashvili S.Sh. Kinetics of crack formation in porous silicon. *Semiconductors*. 2012, Vol. 46, No. 2, pp. 137 – 140. https://doi.org/10.1134/S1063782612020108.

23 Błaszczyński T., Ślosarczyk A., Morawski M. Synthesis of silica aerogel by supercritical drying method. Procedia eng. 2013, Vol. 57, pp. 200 – 206. https://doi.org/10.1016/j.proeng.2013.04.028.

24 Chae H.K., Siberio-Pérez D.Y., Kim J., et al. A route to high surface area,porosity and incusion of large molecules in crystals. *Nature*. 2004, Vol. 427, pp. 523 – 527. https://doi.org/10.1038/nature02311.

25 Chuvil'deev V.N., Nokhrin A.V., Kopylov V.I., et al. Spark plasma sintering for high-speed diffusion bonding of the ultrafine-grained near-α Ti–5Al–2V alloy with high strength and corrosion resistance for nuclear engineering. *J. mater. sci*. 2019, Vol. 54, pp. 14926 – 14949. https://doi.org/10.1007/s10853-019-03926-6.

26 Ganeriwala R., Zohdi T.I. Multiphysics modeling and simulation of selective laser sintering manufacturing processes. *Procedia CIRP*. 2014, Vol. 14, pp. 299 – 304. https://doi.org/10.1016/j.procir.2014.03.015.

27 Berner M.K., Zarko V.E., Talawar M.B. Nanoparticles of energetic materials: synthesis and properties (review). *Combust., explos., shock waves*. 2013, Vol. 49, pp. 625 – 647. https://doi.org/10.1134/S0010508213060014.

28 Hakamada M., Mabuchi M. Nanoporous Ni fabricated by dealloying of rolled Ni-Mn sheet. *Procedia eng*. 2014, Vol. 81, pp. 2159 – 2164. https://doi.org/10.1016/j.proeng.2014.10.302.

29 Zhanabaev Z.Zh., Ibraimov M.K., Sagidolda E. Electrical properties of fractal nanofilms of porous silicon. *Eurasian phys. tech. j.* 2013, Vol. 10, No.1, pp. 3 – 6.

30 Shishulin A.V., Fedoseev V.B. On some peculiarities of stratification of liquid solutions within pores of fractal shape. *J. mol. liq*. 2019, Vol. 278, pp. 363 – 367. https://doi.org/10.1016/j.molliq.2019.01.050.

31 Shishulin A.V., Fedoseev V.B. Peculiarities of phase transformations of polymer solutions in deformable porous matrices. *Tech. phys. lett*. 2019, Vol. 45, No. 7, pp. 697 – 699. https://doi.org/10.1134/S1063785019070289.

32 Shishulin A.V., Fedoseev V.B. Stratifying polymer solutions in microsized pores: phase transitions induced by deformation of a porous material. *Tech. phys*. 2020, Vol. 65, No. 3, pp. 340 – 346. https://doi.org/10.1134/S1063784220030238.

33 Magomedov M.N. Size dependence of the shape of a silicon crystal during melting. *Tech. phys. lett*. 2016, Vol. 42, No. 7, pp. 761 – 764. https://doi.org/10.1134/S1063785016070245.

34 Guisbiers G., Buchaillot L. Universal size/shape-dependent law for characteristic temperatures. *Phys. lett. A*. 2009, Vol. 374, pp. 305 – 308. https://doi.org/10.1016/j.physleta.2009.10.054.

35 Guisbiers G. Size-dependent materials properties toward a universal equation. *Nanoscale res. lett.* 2010, Vol. 5, No. 1132. https://doi.org/10.1007/s11671-010-9614-1.

36 Guisbiers G., Abudukelimu G. Influence of nanomorphology of the melting and catalytic properties of convex polyhedral nanoparticles. *J. nanopart. res*. 2013, Vol. 15, No. 1431. https://doi.org/10.1007/s11051-013-1431-x.

37 Aqra F., Ayyad A. Surface free energy of alkali and transition metal nanoparticles. *Appl. surf. sci*. 2014, Vol. 324, pp. 308 – 313. https://doi.org/10.1016/j.apsusc.2014.07.004.

38 Potapov A.A. On the issues of fractal radio electronics: Processing of multidimensional signals, radiolocation, nanotechnology, radio engineering elements and sensors. *Eurasian phys. tech. j.* 2018, Vol. 15, No. 2, pp. 5 – 15.

39 Fedoseev V.B., Potapov A.A., Shishulin A.V., Fedoseeva E.N. Size and shape effect on the phase transitions in a small system with fractal interphase boundaries. *Eurasian phys. tech. j.* 2017, Vol. 14, No.1, pp. 18 – 24.

40 Shishulin A.V., Fedoseev V.B., Shishulina A.V. Melting behavior of fractal-shaped nanoparticles (the example of Si-Ge system). *Tech. phys.* 2019, Vol. 64, No. 9, pp. 1343 – 1349. https://doi.org/10.1134/S1063784219090172.

41 Shishulin A.V., Fedoseev V.B. On mutual solubility in submicron-sized particles of the Pt-Au catalytic system. *Kinet. catal*. 2019, Vol. 60, No. 3, pp. 315-319. https://doi.org/10.1134/S0023158419030121.

42 Shishulin A.V., Potapov A.A., Fedoseev V.B. *Phase equilibria in fractal core-shell nanoparticles of* $Pb_5(VO_4)_3Cl$ – $Pb_5(PO_4)_3Cl$ *system: the influence of size and shape*. In: Z. Hu, S. Petoukhov, M. He (eds.). Advances in artificial systems for medicine and education II. Cham., Springer. 2020, pp. 405 – 413. https://doi.org/10.1007/978-3-030-12082-5_37.

43 Fedoseev V.B., Shishulin A.V. On the size distribution of dispersed fractal particles. *Tech. phys*. 2021, Vol. 66, No. 1, pp. 34 – 40. https://doi.org/10.1134/S1063784221010072.

44 Attarian Shandiz M. Effective coordination number model for the size dependency of physical properties of nanocrystals. *J. phys.: condens. matter*. 2008, Vol. 20, No. 325237. https://doi.org/10.1088/0953-8984/20/32/325237.

45 Len'shina N.A., Arsenyev M.V., Shurygina M.P., et al. Photoreduction of o-benzoquinone moiety in mono- and poly(quinone methacrylate) and on the surface of polymer matrix pores. *High energy chem*. 2017, Vol. 51, pp. 209 – 214. https://doi.org/10.1134/S0018143917030080.

46 Bronstein L.M., Sidorov S.N., Valetskii P.M. Nanostructured polymeric systems as nanoreactors for nanoparticle formation. *Russ. chem. rev*. 2004, Vol. 73, No. 5, pp. 501 – 515. https://doi.org/10.1070/RC2004v073n05ABEH000782.

47 Villanueva A., De la Presa P., Alonso J.M., et al. Hyperthermia *hela cell* treatment with silica-coated manganese oxide nanoparticles. *J. phys. chem. C*. 2010, Vol. 114, pp. 1976–1981. https://doi.org/10.1021/jp907046f.

Article accepted for publication 23.04.2021